공학석사 학위논문

Aero-thermo-elastic Effects on Sandwich Panel with Temperature-dependent Shear Correction Factor

온도 의존적 전단 보정 계수를 고려한 샌드위치 패널의 공력-열-탄성학적 연계해석

2022년 12월

서울대학교 대학원

항공우주공학과

강 지 훈

온도 의존적 전단 보정 계수를 고려한 샌드위치 패널의 공력-열-탄성학적 연계해석

Aero-thermo-elastic Effects on Sandwich Panel with Temperature-dependent Shear Correction Factor

지도교수 김 지 환

이 논문을 공학석사 학위논문으로 제출함

2022 년 12 월

서울대학교 대학원

항공우주공학과

강 지 훈

강지훈의 공학석사 학위논문을 인준함

2022 년 12 월

위 원 장 윤군진

부위원장 김지환

위 원 신상준

Abstract

Advanced composite structures are used in aerospace, military, nuclear reactors, chemical plants, and modern architecture. In particular, sandwich panels with honeycomb cores have been developed for specific applications in high-temperature regions. As elevated temperatures affect the properties of composite structures, an asymmetric laminated composite plate model was developed for the thermo-elastic vibration, thermal buckling, post-buckling and limit-cycle oscillation (LCO) analyses with different core-face sheet thickness ratio. The First-order Shear Deformation Theory of Plate (FSDTP), which adopts the shear correction factor (SCF), is used with the consideration of heat conduction and supersonic flow. To derive the SCF, the shear strain energy equality of each layer and that of the composite plate were used in the stress equilibrium equation using temperature-dependent (T-D) material properties. A three-layer composite model with face sheets and core composed of a metal matrix composite (MMC) and a titanium honeycomb was introduced for high temperature applications. For the linear analyses, natural frequencies and critical temperature are derived for the vibration and thermal buckling analyses, respectively. Furthermore, non-linear analyses are held using Newton-Raphson method for

post-buckling analysis and Newmark time iteration method for limit-cycle oscillation. First-order piston theory is considered for the aero-dynamic loads. Diverse case studies are held for the various core-face sheet thickness ratio, aspect ratio, and different fiber directions. The results are compared with those obtained using conventional SCF.

Keyword: Thermo-elastic material properties, Heat conduction, Aero-dynamics, Physical neutral surface, Metal Matrix Composite, Titanium Honeycomb

Student Number: 2020-21216

Table of Contents

List of Tables and Figures

Tables

Figures

List of Nomenclature

$\boldsymbol{A}$	In-plane stiffness matrix
$\boldsymbol{A_d}$	Aerodynamic damping matrix
$\boldsymbol{A_f}$	Aerodynamic influence matrix
$\boldsymbol{A_s}$	Transverse shear stiffness matrix
a	Panel length, width
$\boldsymbol{D}$	Bending stiffness matrix
D_m	Bending rigidity
$\boldsymbol{d}$	Displacement vector
$\boldsymbol{e}$	In-plane strain vector
$\boldsymbol{f}$	External force vector
g_a	Non-dimensional aerodynamic damping parameter
h	Panel thickness
$\boldsymbol{K}$	Linear elastic stiffness matrix
$\boldsymbol{K_{\Delta T}}$	Thermal geometric stiffness matrix
$\boldsymbol{M}$	Mass matrix
$\boldsymbol{M_b}, \boldsymbol{M_{\Delta T}}$	Moment resultant and thermal moment resultant vectors
M_∞	Mach number
$\boldsymbol{N_b}, \boldsymbol{N_{\Delta T}}$	In-plane force and thermal in-plane force resultant vectors
$\boldsymbol{N_1}, \boldsymbol{N_2}$	First-order and second-order nonlinear stiffness matrices
P, P_k	Temperature dependent material properties
$\boldsymbol{P_{\Delta T}}$	Thermal load vector
$\overline{\boldsymbol{Q}}$	Transformed stiffness coefficients matrix
$\boldsymbol{Q_s}$	Transverse shear force resultant vector

T	Temperature in Kelvin unit
T_{cr}	Critical temperature
z_N	Physical neutral surface
V_∞	Airflow speed
$\delta W_{\text{int}}, \delta W_{\text{ext}}$	Internal and external virtual work
α	Thermal expansion coefficient
$\boldsymbol{\gamma}$	Transverse shear strain vector
$\boldsymbol{\epsilon_0}$	In-plane strain vector at the midplane
κ	Heat conduction coefficient
κ_p	Shear correction factor
λ	Non-dimensional aerodynamic pressure
μ	Air-panel mass ratio
ρ	Density
$\boldsymbol{\sigma}$	In-plane stress vector
$\phi_x . \phi_y$	Rotations of the transverse normal in the xz and yz planes
ω^*	Non-dimensional frequency
$\boldsymbol{\chi}$	Curvature strain vector

Subscripts

b	bottom
cr	critical
s	time-independent static
t	time-dependent dynamic
u	top

1. Introduction

Composite laminates have become essential structural elements as they possess higher strength than mono-materials despite their light weight, even at elevated temperatures. Especially, sandwich structures composed with titanium honeycomb core and Metal Matrix Composite (MMC) [1] face sheets exhibit exceptional stiffness and strength. In addition, the honeycomb core allows the structure to withstand bending deflection, and it has a relatively low thermal conductivity and light weight. So, the structures perform outstanding thermal barrier which in turn the sandwich structures are commonly used as the outer skin of space shuttle, military missions, and architecture. Therefore, structural analyses such as vibration, buckling, post-buckling and limit-cycle oscillation are inevitable for the sandwich panel to prevent structure deformation or failure.

For the development of the composite structures, analytical modeling for vibration of the structures have been extensively investigated in past few decades. Liu [2] studied the vibration behavior of laminated composite plates which are subjected to temperature changes. Tong [3] investigated the variations in the natural frequencies of conical shells with the altering fiber directions. In addition, Hachemi [4] presented the free vibration analysis of a laminated square composite plate with complicated cutouts. Furthermore, Ribeiro [5] studied the vibration of laminated composite plates with varied stiffness. Vibration analyses are held by Khatua [6], who held the bending and vibration of multilayer sandwich beams and plates. Wang and Zhang [7] discussed for the free vibration of sandwich panel containing honeycomb core. Further, thermal buckling of sandwich plate analysis are held by Matsunaga [8]. Tran

and Thai [9], also investigated the thermal buckling analysis of functionally graded plates. They showed the difference of analysis method between first-order and third-order deformation theory. Shariyat [10], researched thermal buckling and post-buckling analyses for rectangular composite plates with the consideration of temperature-dependent material properties. Further non-linear analyses are held for Limit-cycle oscillation (LCO). With the aero-dynamic load, the structure vibrates in a constant amplitude in some manner. Lee and Kim [11] held the thermal post-buckling and limit-cycle oscillation under supersonic flow. Song and Li [12] also developed the flutter analysis of lightweight sandwich structures.

For the simplification of calculations and to obtain precise results, the structures are analyzed using the First-order Shear Deformation Theory of Plate (FSDTP), and the shear correction factor (SCF) is considered for the accuracy of the analysis. Puchegger [13] performed experiments using a simple bar, and the results showed the dependence of the SCF on the aspect ratio of structures. Still, the SCF tends to be constant for low aspect ratio structures (less than unity). Bert [14] used the equilibrium equation considering shear strain energy equality based on the neutral surface concept for the asymmetric laminated beam to derive the factor. Especially, the variation of SCF was shown for a bi-modular structure with properties changing through the innate fiber direction.

For the thick plate model, shear has a greater effect on the structures. Lim [15] derived the improved correction factor by matching the deflection obtained using the FSDTP and the Third-order Shear Deformation Theory. The results showed that the aspect ratio largely affects the derivation of the factor. Vlachoutsis [16] adopted the neutral surface concept to reduce the calculation process remarkably, yet the Poisson

ratio was considered constant through the thickness direction, which is affected by high temperature. Further, multilayered laminates have been studied by Isaksson [17], who calculated the factor for the corrugated core structure. Moreover, Pan and Wu [18] researched the shear deformation of the honeycomb core and showed that the contribution of bending deformation was equivalent to the transverse shear effect for the decreased core thickness. Nguyen and Sab [19] obtained the factor for functionally graded material (FGM) plates and found that the prediction of the factor plays an important role in static analysis.

Almost every materials properties are affected by temperature, which is not limited to only high-temperature regions. Thus, interpolation from the given values at several temperature points is conducted to derive material properties at intended temperatures. This so-called curve fitting process, which was performed by Reddy [20] who first introduced the thermal effect on material properties for FGM and the values used for the interpolation was firstly reported in the experiment held by Touloukian [21]. Even the analyses are containing the thermal effect such as temperature-dependent (T-D) material properties, heat conduction etc., the method that contains SCF supposed the factor as temperature-independent (TID).

Considering the high-temperature area, Aklilu [22] considered the thermal effect on carbon, glass, and hybrid polymer composites. Fatemi [23] used temperature-dependent (T-D) material properties to know the thermal effect on the honeycomb core structure. Demirbas [24] considered the temperature effect on the stress and strain of Functionally Graded (FG) rectangular plates in a high-temperature region using finite element method. Papakonstatinou [25] et al. analyzed the material properties of composites at room temperature as well as elevated temperatures and

estimated the less expensive polysialate composites can be a substitute of common materials. Yoo and Kim [26] optimized the design of a smart skin structure using genetic algorithm with the thermal conductivity effect. Matsunaga [27] showed the effect of temperature on the dynamic response of angle-ply laminates using higher-order Shear Deformation Theory.

Some researchers handled the thermal effect on SCF, which is only conducted for the FGMs. Hong [28] reported the variation in the SCF due to volume fraction and temperature for the vibration and deflection analysis of FG shells. Lim and Kim [29] researched thermo-elastic effects on the SCF for three FG beam models, and Lee and Kim [30] derived the T-D SCF for FGM plates using heat transfer. The results showed that temperature highly influences the SCF in the high-thermal region.

However, none of these studies considered the thermal effect on SCF for discrete multi-layered structures. In this study, natural frequencies were derived for the vibration analysis of a laminated composite plate considering the Temperature Dependent Shear Correction Factor (T-D SCF). Specifically, an asymmetric sandwich plate was studied with varying temperature, aspect ratio, and fiber direction. The derivation process was conducted after curve fitting in every temperature range, and the values of the SCF were verified using the previously reported data.

With the T-D SCF consideration, aero-thermo-elastic effect on sandwich panel is analyzed after the research. For the linear analysis, thermal vibration and buckling is shown by deriving natural frequency and critical temperature. Further, non-linear analysis is depicted with thermal post-buckling and limit cycle oscillation (LCO),

with the heat conduction effect. von-Karman strain-displacement relations [31] are considered for the non-linear analysis and First-order Piston theory [32] is used for the aero-dynamic conditions. Verification for the results are shown with the previous researches, and the case studies are held for heat conduction, fiber direction, aspect ratio and thickness ratio difference under T-D SCF.

2. Formulation

The three layered sandwich panel constructed with MMC face sheet and titanium honeycomb core including the physical neutral surface z_N is shown in Figure 1. The thickness of face sheet and core is h_f and h_c. The total thickness is h and the length and width of model are a, respectively.

2.1. Material model

Structures used at high-thermal area change their material properties due to the temperature rise. For the investigation of temperature effects, it is appropriate to use interpolation from material properties at several temperature points [33]. Then the material properties can be expressed as the function of temperature in the second-order polynomial form as:

$$P(T) = P_0 T^2 + P_1 T + P_2 \tag{1}$$

where T is the temperature, and P_0, P_1 and P_2 are constants, which are shown in Table 1. Also, $P(T)$ can be represented as temperature-dependent Young's modulus, Shear Modulus, Poisson's ratio, thermal expansion coefficient density and coefficient of heat transfer as shown in Table 2. Using the above equation, it is possible to derive T-D material properties in the whole temperature range.

Also, z_N is the position neutral surface as [34], and with the consideration of thermal effect, the equation is expressed as:

$$z_N(T) = \frac{\int_{-h/2}^{h/2} z\bar{Q}_{xx}(z,T)dz}{\int_{-h/2}^{h/2} \bar{Q}_{xx}(z,T)dz} = \frac{\frac{1}{2}\sum_{k=1}^{n}\left(\bar{Q}_{xx}(T)\right)_k\left(z_k^2 - z_{k-1}^2\right)}{\sum_{k=1}^{n}\left(\bar{Q}_{xx}(T)\right)_k(z_k - z_{k-1})} \tag{2}$$

2.2. Heat conduction

With the consideration of one-dimensional steady-state heat conduction in thickness direction on three layered sandwich panel, the temperature on position z can be described as:

$$\frac{d}{dz}\left[K(z)\frac{dT}{dz}\right] = 0 \tag{3}$$

where $K(z)$ is the heat conduction coefficient dependent on z. Then, the temperature of each layer can be obtained by solving equation (3) with the boundary conditions. That is,

$$T_1 = T_b = T_{ref},\ T_4 = T_u,\ T_i|_{z=z_i} = T_{i+1}|_{z=z_i},\ K_i\frac{dT_i}{dz}|_{z=z_i} \qquad (i = 2,3,4)$$

where the subscript b and u are the bottom and upper surface, respectively. Note that each interface has the equal temperature value. The temperature distribution of sandwich panel is shown in Fig. 2.

2.3. Constitutive equation

For the analysis of current sandwich panel, First-order Shear Deformation Theory of Plate (FSDPT) is used. The displacement field considering temperature and time-difference are expressed as following:

$$\begin{Bmatrix} u(x,y,z,t,T) \\ v(x,y,z,t,T) \\ w(x,y,z,t,T) \end{Bmatrix} = \begin{Bmatrix} u_0(x,y,t,T) + \left(z - z_N(T)\right)\phi_x(x,y,t,T) \\ v_0(x,y,t,T) + \left(z - z_N(T)\right)\phi_y(x,y,t,T) \\ w_0(x,y,t,T) \end{Bmatrix} \tag{4}$$

where u, v, and w are the displacements in the x, y and z directions. Also, the rotation of the transverse normal in the xz and yz plates is ϕ_x and ϕ_y respectively. The subscript 0 indicates the displacements in mid-plane.

Using the von-Karman large deflection theory, in-plane strain vector $\mathbf{e}$ including nonlinear terms is [31]:

$$\mathbf{e} = \boldsymbol{\epsilon_0} + (z - z_N)\boldsymbol{\chi}$$

$$= \begin{Bmatrix} \epsilon_{xx} \\ \epsilon_{yy} \\ \gamma_{xy} \end{Bmatrix} = \begin{Bmatrix} u_{0,x} + \frac{1}{2}w_{0,x}^2 + (z - z_N)\phi_{x,x} \\ u_{0,y} + \frac{1}{2}w_{0,y}^2 + (z - z_N)\phi_{y,y} \\ u_{0,y} + v_{0,x} + w_{0,x}w_{0,y} + (z - z_N)(\phi_{x,y} - \phi_{y,x}) \end{Bmatrix} \tag{5}$$

where $\boldsymbol{\epsilon_0}$ and $\boldsymbol{\chi}$ are the in-plane strain vector at the mid-plane and the curvature strain vector, respectively.

Further, the transverse shear strain vectors $\boldsymbol{\gamma}$ can be derived as

$$\boldsymbol{\gamma} = \begin{Bmatrix} \gamma_{yz} \\ \gamma_{xz} \end{Bmatrix} = \begin{Bmatrix} w_{0,y} + \phi_y \\ w_{0,x} + \phi_x \end{Bmatrix} \tag{6}$$

Since the thermal stresses are not caused by external load but by the expansion of material under the restrained boundary condition, stress-strain relations are written as:

$$\boldsymbol{\sigma} = [\bar{Q}](\boldsymbol{\epsilon} - \boldsymbol{\alpha}\Delta T) \tag{7}$$

Subsequently, the stresses in the kth layer of laminate is expressed

$$\begin{Bmatrix} \sigma_x \\ \sigma_y \\ \tau_{xy} \end{Bmatrix}_k = \begin{bmatrix} \bar{Q}_{11} & \bar{Q}_{12} & \bar{Q}_{16} \\ \bar{Q}_{12} & \bar{Q}_{22} & \bar{Q}_{26} \\ \bar{Q}_{16} & \bar{Q}_{26} & \bar{Q}_{66} \end{bmatrix}_k \left(\begin{Bmatrix} \epsilon_x \\ \epsilon_y \\ \gamma_{xy} \end{Bmatrix}_k - \Delta T \begin{Bmatrix} \alpha_x \\ \alpha_y \\ \alpha_{xy} \end{Bmatrix}_k \right) \tag{8}$$

Where $[\bar{Q}_{ij}]$ are the transformed stiffness coefficients due to fiber direction and ΔT is the temperature rise.

Further, α_x, α_y and α_{xy} are defined as

$$\alpha_x = \alpha_1 \cos^2\theta + \alpha_2 \sin^2\theta$$

$$\alpha_y = \alpha_1 \sin^2\theta + \alpha_2 \cos^2\theta \tag{9}$$

$$\alpha_{xy} = 2(\alpha_1 - \alpha_2)\sin\theta\cos\theta$$

where α_1 and α_2 are the thermal expansion coefficient in x, y direction, respectively, and θ is the angle ply.

Finally, the in-plane force and moment vector considering the thermal effect can be expressed as following

$$\begin{Bmatrix} \boldsymbol{N_b}(T) \\ \boldsymbol{M_b}(T) \end{Bmatrix} = \begin{bmatrix} \boldsymbol{A}(T) & 0 \\ 0 & \boldsymbol{D}(T) \end{bmatrix} \begin{Bmatrix} \boldsymbol{\epsilon} \\ \boldsymbol{\chi} \end{Bmatrix} - \begin{Bmatrix} \boldsymbol{N_{\Delta T}} \\ \boldsymbol{M_{\Delta T}} \end{Bmatrix} \tag{10}$$

$$\boldsymbol{Q_s} = A_s \boldsymbol{\gamma} \tag{11}$$

where

$$(\boldsymbol{A}(T), 0, \boldsymbol{D}(T)) = \sum_{k=1}^{n} \int_{z_{k-1}}^{z_k} \left(\bar{Q}_{ij}(T)\right)_k (1, 0, (z - z_N)^2)\, dz \quad (i, j = 1,2,6) \tag{12}$$

$$\boldsymbol{A_s} = \sum_{k=1}^{n} \kappa_p(T) \int_{z_{k-1}}^{z_k} \left(\bar{Q}_{ij}\right)_k dz \qquad (i,j = 4,5) \tag{13}$$

where $\kappa_p(T)$ is temperature-dependent shear correction factor (T-D SCF) which detailed derivation process written in Appendix A. Meanwhile, the thermal force $N_{\Delta T}$ and moment $M_{\Delta T}$ vectors are

$$\begin{aligned} &\left(\boldsymbol{N_{\Delta T}}(T), \boldsymbol{M_{\Delta T}}(T)\right) \\ &= \sum_{k=1}^{n} \int_{z_{k-1}}^{z_k} \left(\bar{Q}_{ij}(T)\right)_k \boldsymbol{\alpha}_k (1, z - z_N) \Delta T(z) dz \qquad (i,j = 1,2,6) \end{aligned} \tag{14}$$

In addition, $\boldsymbol{\alpha}$ are defined as $\alpha = \left[\alpha_x(z), \alpha_y(z), 0\right]^T$

2.4. Aerodynamic pressure by supersonic flow

For the structures are considerably applied for the supersonic condition, aerodynamic external forces are also studied. Using the first-order piston theory [32], the range of $\sqrt{2} < M_\infty < \sqrt{5}$ is considered:

$$p_a(x,y,t) = -\frac{\rho_a V_\infty^2}{\sqrt{M_\infty^2 - 1}} \left\{ w_{,x} + \left(\frac{M_\infty^2 - 2}{M_\infty^2 - 1}\right) \frac{1}{V_\infty} w_{,t} \right\} = -(\lambda \frac{D_m}{a^3} w_{,x} + \frac{g_a}{\omega_0} \frac{D_m}{a^4} w_{.t}) \tag{15}$$

where V_∞, M_∞ and ρ_a are the air flow speed, Mach number and air density, respectively. Again, non-dimensional aerodynamic pressure is expressed as

$$\lambda = \frac{\rho_a V_\infty^2 a^3}{\beta D_m} \tag{16}$$

where D_m is the bending rigidity directed as follows

$$D_m = \frac{Eh^3}{12(1 = \nu^2)} \tag{17}$$

Also, the non-dimensional aerodynamic damping parameter is

$$g_a = \frac{\rho_a V_\infty (M_\infty^2 - 2)}{\beta^3 \rho_m h \omega_0} \tag{18}$$

where $\omega_0 = \sqrt{\frac{D_m}{\rho_m h a^4}}$ is the convenient reference frequency, and $\beta = \sqrt{M_\infty^2 - 1}$ is the aerodynamic pressure parameter. Then, for the high enough Mach number($M_\infty \gg 1$), Eq. (18) is approximated as [35]

$$g_a = \sqrt{\frac{\mu}{M_\infty}\lambda} \tag{19}$$

where μ is the air-mass ratio defined as $\mu = \rho_a a / \rho_m h$ [36].

2.5. Governing equations

To derive the equation of motion with thermal and aerodynamic pressure, the principle of virtual work is applied

$$\delta W = \delta W_{int} - \delta W_{ext} = 0 \tag{20}$$

where δW_{int} and δW_{ext} are the internal and external virtual works, respectively. The internal work is given as

$$\begin{aligned} \delta W_{int} &= \int_V \delta \boldsymbol{e}^T \boldsymbol{\sigma} dV \\ &= \int_A [\delta \boldsymbol{\epsilon}^T \boldsymbol{N} + \delta \boldsymbol{\chi}^T \boldsymbol{M} + \delta \boldsymbol{\gamma}^T \boldsymbol{Q}] dA \end{aligned} \tag{21}$$

$$= \delta \boldsymbol{d}^T \left[\boldsymbol{K} - \boldsymbol{K_{\Delta T}} + \frac{1}{2}\boldsymbol{N_1} + \frac{1}{3}\boldsymbol{N_2} \right] \boldsymbol{d} - \delta \boldsymbol{d^T P_{\Delta T}}$$

here, $\boldsymbol{\sigma} = \{\sigma_x, \sigma_y, \tau_{xy}\}^T$, $\boldsymbol{e} = \{\epsilon_x, \epsilon_y, \gamma_{xy}\}^T$ and $\boldsymbol{d} = \{u \;\; v \;\; w \;\; \phi_x \;\; \phi_y\}$ denotes the stress, strain, displacement vector, and $\boldsymbol{K}$, $\boldsymbol{K_{\Delta T}}, \boldsymbol{N_1}, \boldsymbol{N_2}$ and $\boldsymbol{P_{\Delta T}}$ represent the linear stiffness, thermal stiffness, first-order nonlinear stiffness, the second-order nonlinear stiffness and the thermal load vectors, respectively.

While, the external virtual work is given by

$$\delta W_{ext} = \\ -\int_A \begin{bmatrix} I_0(\ddot{u}\delta u + \ddot{v}\delta v + \ddot{w}\delta w) + I_1\left(\ddot{u}\delta\phi_x + \ddot{\phi}_x\delta u + \ddot{v}\delta\phi_y + \ddot{\phi}_y\delta v\right) \\ +I_2\left(\ddot{\phi}_x\delta\phi_x + \ddot{\phi}_y\delta\phi_y\right) + p_a\delta w \end{bmatrix} dA \tag{22}$$

$$= -\delta \boldsymbol{d^T M \ddot{d}} + \delta \boldsymbol{d^T f}$$

where $\boldsymbol{M}$ and $\boldsymbol{f}$ are global mass matrix and external force vector. And for the external virtual work, moments of inertia are defined as $(I_0, I_1, I_2) = \int_{-h/2}^{h/2} \rho(1, z, z^2) dz$.

Now the last term of Eq. (22) can be substituted as following with the adjustment of aerodynamics:

$$\begin{aligned} \delta \boldsymbol{d^T f} &= \int_A p_a \delta w dA = -\int_A \left(\frac{g_a}{\omega_0} \frac{D_m}{a^4} w_{,t} + \lambda \frac{D_m}{a^3} w_{,x} \right) \delta w dA \\ &= -\delta \boldsymbol{d^T} \left(\frac{g_a}{\omega_0} \boldsymbol{A_d} \dot{\boldsymbol{d}} + \lambda \boldsymbol{A_f d} \right) \end{aligned} \tag{23}$$

where $\boldsymbol{A_d}$ and $\boldsymbol{A_f}$ are the aerodynamic damping matrix and aerodynamic influence matrix, respectively.

Then the external virtual work in Eq. (22) can be represented as

$$\delta W_{ext} = -\delta \boldsymbol{d}^{\boldsymbol{T}} \left(\boldsymbol{M}\ddot{\boldsymbol{d}} + \frac{g_a}{\omega_0} \boldsymbol{A_d}\dot{\boldsymbol{d}} + \lambda \boldsymbol{A_f}\boldsymbol{d} \right) \tag{24}$$

By substituting Eqs. (21) and (24) into Eq. (20), the equation of motion are obtained as

$$\boldsymbol{M}\ddot{\boldsymbol{d}} + \frac{g_a}{\omega_0} \boldsymbol{A_d}\dot{\boldsymbol{d}} + \left(\boldsymbol{K} - \boldsymbol{K_{\Delta T}} + \frac{1}{2}\boldsymbol{N_1} + \frac{1}{3}\boldsymbol{N_2} + \lambda \boldsymbol{A_f} \right) \boldsymbol{d} = \boldsymbol{P_{\Delta T}} \tag{25}$$

2.6. Solutions of equations

2.6.1 Linear analysis

To solve the linear analyses of thermal vibration and buckling from Eq. (25), the formulation is assumed to be

$$\boldsymbol{M}\ddot{\boldsymbol{d}} + (\boldsymbol{K} - \boldsymbol{K_{\Delta T}})\boldsymbol{d} = \boldsymbol{P_{\Delta T}} \tag{26}$$

In here, natural frequency is obtained by solving the Weigenvalue problem as

$$\boldsymbol{M}\ddot{\boldsymbol{d}} + (\boldsymbol{K} - \boldsymbol{K_{\Delta T}})\boldsymbol{d} = 0 \tag{27}$$

while the thermal buckling problem is solved by changing the Eq. (27) as

$$(\boldsymbol{K} - \boldsymbol{K_{\Delta T}})\boldsymbol{d} = \boldsymbol{0} \tag{28}$$

2.6.2 Nonlinear analysis

The first step to solve the nonlinear problem from Eq. (25) is dividing the displacement vector $\boldsymbol{d}$ into static part $(\boldsymbol{d_s})$ and dynamic part $(\boldsymbol{\Delta d_t})$ as

$$\boldsymbol{d} = \boldsymbol{d_s} + \boldsymbol{\Delta d_t} \tag{29}$$

where the subscript $\boldsymbol{s}$ and $\boldsymbol{t}$ denote the static and dynamic terms, respectively. Then, the static nonlinear equation is obtained as following:

$$\left(\boldsymbol{K}-\boldsymbol{K}_{\boldsymbol{\Delta T}}+\frac{1}{2}\boldsymbol{N}_{\boldsymbol{1}}+\frac{1}{3}\boldsymbol{N}_{\boldsymbol{2}}+\lambda\boldsymbol{A}_{\boldsymbol{f}}\right)\boldsymbol{d}_{\boldsymbol{s}}=\boldsymbol{P}_{\boldsymbol{\Delta T}} \tag{30}$$

Using the Newton-Raphson iterative method [37], the nonlinear post-buckling deflection is obtained.

While the time dependent part $\boldsymbol{\Delta d_t}$ is used to form the dynamic nonlinear equation as

$$\boldsymbol{M}\boldsymbol{\Delta}\ddot{\boldsymbol{d}}_{\boldsymbol{t}}+\frac{g_a}{\omega_0}\boldsymbol{A}_{\boldsymbol{d}}\boldsymbol{\Delta}\dot{\boldsymbol{d}}_{\boldsymbol{t}}+\begin{pmatrix}\boldsymbol{K}-\boldsymbol{K}_{\boldsymbol{\Delta T}}+\boldsymbol{N}_{\boldsymbol{1s}}+\boldsymbol{N}_{\boldsymbol{2s}}\\+\lambda\boldsymbol{A}_{\boldsymbol{f}}+\boldsymbol{N}_{\boldsymbol{2st}}+\frac{1}{2}\boldsymbol{N}_{\boldsymbol{1t}}+\frac{1}{3}\boldsymbol{N}_{\boldsymbol{2t}}\end{pmatrix}\boldsymbol{\Delta d}_{\boldsymbol{t}} \tag{31}$$

$$=\boldsymbol{P}_{\boldsymbol{\Delta T}}$$

where $\boldsymbol{N_{1t}}$, $\boldsymbol{N_{2t}}$ and $\boldsymbol{N_{2st}}$ are the time dependent nonlinear stiffness matrices. Eq. (31) is the equation of motion for limit cycle oscillation or flutter behaviors. By adopting Newmark method [38],the time domain response of plate model is obtained.

3. Numerical Results and Discussion

3.1 Code verification

For the validation of the code used to analyze the T-D SCF for the three layered sandwich laminate using the neutral surface, the material properties reported by Whitney [39] and Vlachoutsis [16] were used, and the results are shown in Table 1. Before calculating the T-D SCF, code verification was performed by comparing the value derived using the material properties at room temperature. The model was a symmetric three-layered sandwich structure, and the detailed material properties of each layer were reported by Whitney [39]. As shown in Table 2, the TID SCF in the *x*-direction of the sandwich structure calculated by Whitney was 0.4098, which is almost the same as that found in this work (0.4094), and the factor for the *y*-direction was obtained as 0.6724, which is similar to that reported by Whitney (0.6915).

After the verification of the SCF, the vibration analysis considering the T-D SCF is also held following the code verification of vibration. To verify the result in this paper, non-dimensional natural frequencies $\Omega = \omega a^2/(h\sqrt{E_2})$ for the temperature independent case are compared with the research reported by Matsunaga [27]. The results shown in Table 3 gives a great agreement with those obtained using the proposed method.

3.2 Curve-fitting process

In this section, the T-D SCFs integrated into actual models are investigated

using numerical calculations. T-D material properties are calculated from the previously reported data [40].

The detailed research is conducted at three different temperatures; consequently, the properties in every temperature range can be calculated for up to 1100 K, which is the service temperature of the titanium alloy honeycomb [41]. Using equation (1), analysis can be conducted for the given core-face sheet thickness ratio, top bottom face sheet thickness ratio, and face sheet fiber direction.

3.3 Temperature-dependent Shear Correction Factor

3.3.1 T-D SCF for Symmetric Structures

Considering the thermal effects on the material properties of the titanium honeycomb core and MMC face sheet shown in Table 1, we can conclude that the SCF is a thermo-elastic parameter. The temperature rises from room temperature (300 K) to the service temperature, 1100 K (Ref [41]). And the two real model types with different fiber angles suggested by Ko [40] with $h = 30.48[mm], h_c = 29.667[mm], h_{f1} = 04064[mm]$, and $h_{f2} = 0.4064[mm]$ (thicknesses of the total structure, core, top, and bottom face sheets, respectively) were studied, as shown in Fig. 1. The MMC face sheet itself was a composite constructed using four fiber-reinforced metals, and its material properties were found considering it as one material using the rule of mixture. In other words, four layers constructing the MMC had individual properties, but for the calculation, it was considered as one material, which had one material property. For the diversity of analysis, two other types were

considered, and the difference was the stacking sequence of the fiber direction in the MMC face sheet: Type I [90°/0°/0°/90°] and Type II [45°/-45°/-45°/45°]. The material properties were given by Gruttmann [42], and the values of plane stress-reduced elastic constants Q_f, Q_c and shear modulus G_f, G_c are also represented, and the indices *f* and *c* indicate the face sheet and the core material.

First, for type I, the value of the T-D SCF rises proportionately with temperature, as shown in Fig. 3a. Both the *x* and *y* directions showed the increasing value, where the *x* value increased to 0.3323 at 930 K, which differs about 18.68% compared to the temperature independent value of 0.28. Also, for the *y* direction, the maximum value was 0.2881 at 987 K, which differs about 86.71%. Next, for type II shown in Fig. 2b, the maximum values of in the *x* and *y* directions were 0.2602 at 445 K and 0.193 at 736 K, respectively. When the material is heated, the material becomes softer, and the value of the T-D SCF decreases. For both type I and II, the factor increases for the appointed temperature and decreases as the temperature rises. At the same time, based on the curve fitting process using the different values at three different temperatures, Fig. 3 shows that the shape is a convex function. Note that the SCF is bigger in the *x* direction than in the *y* direction because of the larger shear modulus.

By changing the ratio of the honeycomb core thickness to the total thickness, the SCF values can be found, as shown in Fig. 4. The ratio of the titanium core thickness to the total thickness varied from 0.5 to 0.95 as the temperature increased from 300 K to 1100 K. When the core thickness increases, the SCF increases rapidly in both types. Since the property of the thick layer is dominant in the whole composite, the titanium honeycomb affects the SCF value, although titanium itself has a TID

material property. Fig. 4a shows the SCF rise due to the core-face sheet thickness variation for type I. For the same temperature condition, κ increases slightly, and as the thickness increases continuously and exceeds 0.7, κ increases rapidly. Subsequently, the thermal effect shows that for type I, the factor increases up to 0.3461 at 966 K for a thickness ratio of 0.95. Similar results can be seen for type II, Fig. 4b (the biggest factor is 0.2683 at 421 K for a thickness ratio of 0.95).

3.3.2 T-D SCF for Asymmetric Structures

The above results are given for symmetric structures, where the mid-plane and the neutral surface are the same. In this section, the structure is considered asymmetric by varying the thicknesses of the top and bottom face sheets, and the thickness ratio is denoted by $= \frac{h_{f1}}{h_{f2}}$.

Now, the derivation process for the three-layered laminate is shown in this section, including the neutral surface which, by substituting 3 into *n* from equation (2). That is:

$$z_{N1} = \frac{\frac{1}{2}\sum_{k=1}^{3}(Q_1)_k(z_k^2 - z_{k-1}^2)}{\sum_{k=1}^{3}(Q_1)_k\,(z_k - z_{k-1})} \tag{32}$$

where z_0 is $-\frac{h}{2}$, and z_3 denotes $\frac{h}{2}$.

Fig. 5 shows the T-D SCF increases for both types due to temperature rise and top-to-bottom face sheet ratio difference. To begin with the type I, the factor appears its minimum value from 0.149 at face sheet ratio 1, which is symmetric condition, at

room temperature (300 K). Continually, T-D SCF turns out to be 0.4764 at a top-to-bottom ratio of 0.8273 at 1100 K. Second, Fig. 5b shows the results of type II, which has a minimum value of 0.05032 at face sheet ratio 1 in 300 K, whereas it is 0.3917 at a ratio of 0.2364 in 1100 K. These results show that the SCF becomes larger with temperature rise along with the face sheet thickness ratio increases.

3.4 Thermo-elastic linear analysis

Linear and non-linear analyses of sandwich panel composed of titanium honeycomb core and MMC face sheet are performed and compared with the different conditions. Three layered composite which is two face sheets and one honeycomb core is analyzed. As described in Fig. 1, the thickness of face sheet and core are 15mm and 30mm, respectively. The temperature-dependent material properties are listed up in Table 1. Also, the boundary condition are used as

Simply supported boundary condition (SS).

$v = w = \phi_y = 0$ when $x = 0, a$

$u = w = \phi_x = 0$ when $y = 0, a$

3.4.1 Vibration behavior

In this part, natural frequencies are derived due to the aspect ratio change. Table 4 shows the natural frequencies of different temperature, aspect ratio, and fiber directions($[90^\circ/0^\circ]_s$, $[45^\circ/-45^\circ]_s$). Minimum value of non-dimensional natural frequency 11603 can be found at a/h 10 in 300 K. As the aspect ratio increases with the constant temperature condition, the natural frequency increases to the maximum

value of 24561 since the structure becomes thinner. For the different fiber direction, Type I in Table 4a shows a slightly lower frequency compared to Type II in Table 4b, and the differences may occur from material stiffness variations.

3.4.2 Buckling behavior

Thermal buckling behavior is analyzed by deriving critical buckling temperature. That is, the temperature when natural frequency becomes zero. From Table 5, code verification is held by obtaining critical temperature compared to Matsunaga [8], and shows good agreement. Table 6 exhibits the critical temperature under different temperature condition and aspect ratio change. As the ratio increases, the model buckles in the lower temperature. Also, for the T-D SCF consideration, buckling occurs earlier compared to the TID condition. This means the change of shear correction factor effects the buckling temperature. Table 8 represents the critical temperature when aero-dynamic load is applied. When the load is larger, the buckling temperature increases, and for the high load more than 600, T-D SCF condition denotes the higher critical temperature than TID condition.

3.5 Aero-thermo-elastic nonlinear analysis

In the preceding step, linear studies of vibration and buckling are examined. Natural frequencies and critical buckling temperatures are determined under the heat conduction condition. Henceforth, nonlinear analyses of post-buckling and limit-cycle oscillation are conducted from the Eqs. (30-31).

3.5.1 Post-buckling behavior

After the buckling situation, when the temperature increases continuously, the model restrained by boundary condition deforms. This is so-called post-buckling which is calculated by Newton-Raphson method and the central displacement of model is researched. To verify the results in this study, the work held by Averill and Reddy [43] is compared. The value described in Fig. 6 shows the great agreement of current code and previous work [43].

Then, the central deflection difference is investigated for the sandwich composite and the T-D SCF consideration under the heat conduction condition. As shown in Fig. 7, the deflection occurs about 20% larger in T-D SCF application than the TID SCF. This means that for the real condition, the structure should me models more strictly since it bends larger than expected.

3.5.2 Limit Cycle Oscillation

The limit-cycle oscillations (LCO) with structural damping are discussed in this section. LCO is due to the geometrical non-linearity of structures, and is well known that the LCO without a catastrophic failure occurs after a critical flutter point, but results in a fatigue failure of the structures. The calculation is held for the same structure in linear analysis. With Newmark time iteration method, and the time step is 0.1ms is used. Additionally, the thickness ratio is $a/h = 100$.

In Fig. 8, flutter research under uniform temperature and heat conduction conditions are described. The aerodynamic pressure is loaded as 1400 in both cases. For the case of heat conduction, flutter motion occurs slower than the uniform condition. However, the limit-cycle amplitude is larger in this case. Several case studies for heat conduction condition are held subsequently. Fig. 9 shows the flutter

motion with T-D SCF and TID SCF. Dynamic pressure is still loaded as 1400, and other conditions are the same except the shear correction consideration. Flutter occurs slower in T-D SCF but the amplitude is similar for both case. The analysis for the temperature change can be seen in, Fig. 10. One has the temperature condition as $\Delta T = \Delta T_{cr}$, and the other is 10 times smaller as $\Delta T = \Delta T_{cr}/10$. The figure represents the great difference of motion and amplitude. When the temperature is higher, limit-cycle occurs earlier and larger. Results in the case of larger aerodynamic load are shown in Fig. 11. Two different types of load (λ) is shown as 1400 and 1600. Flutter occurs faster and the amplitude is bigger for the larger aerodynamic load. This is similar with the higher temperature condition.

4. Conclusion

Using the FSDTP, the error compensation was conducted by considering the transverse effect and rotary inertia, and the SCF was calculated. In this work, to obtain the temperature dependent shear correction factor, thermo-elastic properties are considered. Three other parameters, the thermal effect, core-face sheet thickness ratio, and top-bottom face sheet ratio, affected the T-D SCF. The top-bottom face sheet ratio makes the structure asymmetric, which subsequently introduces the neutral surface concept. When the temperature increases, the Young's modulus decreases and continuously, the T-D SCF changes, as shown in Fig. 3-5.

For the vibration analysis, thermal expansion due to temperature increase changes the T-D SCF, which in turn affects the non-dimensional natural frequency. Irrespective of the fiber direction, when the temperature increases, the SCF inclines, and the eigenvalue becomes smaller compared to the value derived from the TID SCF. Also, when the core thickness is larger compared to the face sheet, the natural frequency becomes smaller. For the buckling analyses, the critical temperature is higher under the heat conduction and T-D SCF condition. With the aerodynamic consideration, the temperature increases as the load rises. Non-linear analyses are also researched. The buckling central deflection becomes larger with the T-D SCF. Lastly, limit-cycle oscillation is researched with two parameters: time, limit-cycle amplitude. When T-D SCF is considered, it takes longer time to reach LCO. Under the lower temperature, LCO occurs slower and smaller. Further, with the higher aerodynamic loads, the same results is derived with the different heat conditions.

Finally, using the T-D SCF shows the considerable difference between vibration, buckling, post-buckling and limit-cycle oscillation. Therefore, it is clear to consider the aero-thermo-elastic effect to analyze models.

References

[1] Kaczmar JW, Pietrzak K, Âski. The production and application of metal matrix composite materials

[2] Liu CF, Huang CH. Free vibration of composite laminated plates subjected to temperature changes. *Computers and Structures* 1996; 60: 95–101.

[3] Tong L. Free vibration of composite laminated conical shells. *International Journal of Mechanical Sciences* 1993; 35: 47–61.

[4] Hachemi M, Hamza-Cherif SM. Free vibration of composite laminated plate with complicated cutout. *Mechanics Based Design of Structures and Machines* 2019

[5] Ribeiro P, Akhavan H. Non-linear vibrations of variable stiffness composite laminated plates. *Composite Structures* 2012; 94: 2424–2432.

[6] Khatua TP, Cheungt YK. Bending and vibration of multilayer sandwich beams and plates. *International Journal For Numerical Methods in Engineering* 1973; 6: 11-24

[7] Wang Y jing, Zhang Z jia, Xue X min, et al. Free vibration analysis of composite sandwich panels with hierarchical honeycomb sandwich core. *Thin-Walled Structures* 2019; 145..

[8] Matsunaga H. Thermal buckling of cross-ply laminated composite and sandwich plates according to a global higher-order deformation theory. *Composite Structures* 2005; 68: 439–454.

[9] Tran L v., Thai CH, Nguyen-Xuan H. An isogeometric finite element formulation for thermal buckling analysis of functionally graded plates. *Finite Elements in Analysis and Design* 2013; 73: 65–76.

[10] Shariyat M. Thermal buckling analysis of rectangular composite plates with temperature-dependent properties based on a layerwise theory. *Thin-Walled Structures* 2007; 45: 439–452.

[11] Lee SL, Kim JH. Thermal post-buckling and limit-cycle oscillation of functionally graded panel with structural damping in supersonic airflow. *Composite Structures* 2009; 91: 205–211.

[12] Song ZG, Li FM. Flutter and buckling characteristics and active control of sandwich panels with triangular lattice core in supersonic airflow. *Composites part B: Engineering* 2017; 108: 334–344.

[13] Puchegger S, Bauer S, Loidl D, et al. Experimental validation of the shear correction factor. *Journal of Sound Vibration* 2003; 261: 177–184.

[14] Bert CW, Gordaninejad F. Transverse Shear Effects in Bimodular Composite Laminates. *Journal of Composite Materials* 1983; 17: 282–298.

[15] Lim TC. Improved shear correction factors for deflection of simply supported very thick rectangular auxetic plates. *International Journal of Mechanical and Materials Engineering* 2016; 11:13

[16] Vlachoutsis S. Shear correction factors for plates and shells. *International Journal for Numerical Methods in Engineering* 1992; 33:1537-1552

[17] Isaksson P, Krusper A, Gradin PA. Shear correction factors for corrugated core structures. *Composite Structures* 2007; 1: 123–130.

[18] Pan SD, Wu LZ, Sun YG. Transverse shear modulus and strength of honeycomb cores. *Composite Structures* 2008; 84: 369–374.

[19] Nguyen T-K, Sab K, Bonnet G. Shear Correction Factors for Functionally Graded Plates. *Mechanics of Advanced Materials and Structures* 2007; 14: 567–575.

[20] Reddy JN, Chin CD. Thermomechanical analysis of functionally graded cylinders and plates. *Journal of Thermal Stresses* 2007; 21: 593–626.

[21] Touloukian. Y. S. Thermophysical Properties of High Temperature Solid Materials. *Defense Technical Information Center* 1966.

[22] Aklilu G, Adali S, Bright G. Temperature effect on mechanical properties of carbon, glass and hybrid polymer composite specimens. *International Journal of Engineering Research in Africa* 2018; 39: 119–138.

[23] Fatemi J, Lemmen MHJ. Effective Thermal/Mechanical Properties of Honeycomb Core Panels for Hot Structure Applications. *J Spacecr Rockets* 2009; 46: 514–525.

[24] Demirbas MD. Thermal stress analysis of functionally graded plates with temperature-dependent material properties using theory of elasticity. *Composites part B: Engineering* 2017; 131: 100–124.

[25] Papakonstantinou CG, Balaguru P, Lyon RE. Comparative study of high temperature composites. *Composites part B: Engineering* 2001; 32: 637–649.

[26] Yoo K-K, Kim J-H. Optimal Design of Smart Skin Structures for Thermo-Mechanical Buckling and Vibration using a Genetic Algorithm. *Journal of Thermal Stresses* 2011; 34: 1003–1020.

[27] Matsunaga H. Free vibration and stability of angle-ply laminated composite and sandwich plates under thermal loading. *Composite Structures* 2007; 77: 249–262.

[28] Hong CC. Varied effects of shear correction on thermal vibration of functionally graded material shells. *Cogent Engineering* 2014; 1: 938430.

[29] Lim TK, Kim JH. Thermo-elastic effects on shear correction factors for functionally graded beam. *Composites part B: Engineering* 2017; 123: 262–270.

[30] Lee SH, Lim TK, Kim JH, Kim JH. Temperature-dependent shear correction factor with heat transfer based on micromechanical properties for FGM plates. *Thin-walled structures 181* 2022; 110095.

[31] Reddy JN. Mechanics of laminated composite plates and shells*: theory and analysis*. CRC press, 2004.

[32] Dowell EH. Nonlinear oscillations of a fluttering plate. *AIAA Journal* 1966; 4: 1267–1275.

[33] K. Williams, Jackson RH. Compressive and shear buckling analysis of metal matrix composite sandwich panels under different thermal environments. *Composite Structures* 1993; 25: 227–239.

[34] Vlachoutsis S. Shear correction factors for plates and shells. *International Journal of Numerical Methods in Engineering* 1992; 33: 1537–1552.

[35] Liao CL, Sun YW. Flutter analysis of stiffened laminated composite plates and shells in supersonic flow. *AIAA Journal* 1993; 31: 1897–1905.

[36] Prakash T, Ganapathi M. Supersonic flutter characteristics of functionally graded flat panels including thermal effects. *Composite Structures* 2006; 72: 10–18.

[37] Na KS, Kim JH. Thermal postbuckling investigations of functionally graded plates using 3-D finite element method. *Finite Elements in Analysis and Design* 2006; 42: 749–756.

[38] Hashamdar H, Ibrahim Z, Jameel M. Finite element analysis of nonlinear structures with Newmark method. *International Journal of the Physical Sciences* 2011; 6: 1395–1403.

[39] Whitney JM. Stress Analysis of Thick Laminated Composite and Sandwich Plates. *Journal of Composite Materials* 1972; 6

[40] K. William L, Jackson. Raymond H. Compressive and shear buckling analysis of metal matrix composite sandwich panels under different thermal environments. *Composite Structures 25* 1993; 227-239

[41] Advanced Materials Technology. High temperature Titanium alloys. *Advanced Materials Technology*, 2014

[42] Gruttmann F, Wagner · W, Wagner BW. Shear correction factors for layered plates and shells. *Computational Mechanics* 2017; 59: 129–146.

[43] Averill RC, Reddy JN. Thermomechanical postbuckling analysis of laminated composite shells. *AIAA* 1993; 351–360.

[44] Chow TS. On the Propagation of Flexural Waves in an Orthotropic Laminated Plate and Its Response to an Impulsive Load. *Journal of Composite Materials* 1971; 5: 306-319

Table 1. Temperature-dependent material properties of the Sandwich Panel

	Metal Matrix Composite [90°]	Metal Matrix Composite [45°]
E_1	$10140T^2 - 8.808e^7T + 1.834e^{11}$[Pa]	$3490T^2 - 1.239e^7T + 1.82e^{11}$[Pa]
E_2	$10140T^2 - 8.808e^7T + 1.834e^{11}$[Pa]	$3490T^2 - 1.239e^7T + 1.82e^{11}$[Pa]
ν_{12}	$-8.532\mathrm{e}^{-8}T^2 - 1.331e^{-5}T + 0.2482$	$2.117\mathrm{e}^{-8}T^2 + 1.106e^{-5}T + 0.2756$
G_{12}	$4847T^2 - 5.696\mathrm{e}^7T + 7.254e^{10}$[Pa]	$5611T^2 - 3.2944\mathrm{e}^7T + 7.322e^{10}$[Pa]
G_{13}	$4847T^2 - 5.696\mathrm{e}^7T + 7.254e^{10}$[Pa]	$5611T^2 - 3.2944\mathrm{e}^7T + 7.322e^{10}$[Pa]
G_{23}	$4847T^2 - 5.696\mathrm{e}^7T + 7.254e^{10}$[Pa]	$5611T^2 - 3.2944\mathrm{e}^7T + 7.322e^{10}$[Pa]
α	$23e^{-6}$/°K	$23e^{-6}$/°K
ρ	3200kg/m^3	3200kg/m^3
k	59W/mK	59W/mK

	Titanium Honeycomb
E_1	110.3161GPa
E_2	110.3161GPa
ν_{12}	0.31
G_{12}	0.6e^9
G_{13}	$-988.8T^2 + 2.329e^5T + 1.454e^9$
G_{23}	$-1695T^2 + 2.071e^6T + 1.878e^8$
α	$2.97e^{-6}$/°K
ρ	4540kg/m^3
k	21.9W/mK

Table 2. Verification of the TID SCF in x and y direction

SCF	**Whitney** [39]	**Present**	**Difference [%]**
$\boldsymbol{\kappa_1}$	0.4098	0.4094	0.04%
$\boldsymbol{\kappa_2}$	0.6915	0.6724	-1.91%

Table 3. Verification of Non-dimensional natural frequencies of the composite plate

a/h	**10**	**20**	**50**	**100**
Present	15.057	17.580	18.600	18.764
Matsunaga	15.153	17.628	18.600	18.804

Table 4 Non-dimensional natural frequencies with different aspect ratio

(a) with fiber direction $[90/0]_s$

a/h	**10**	**20**	**50**	**100**
T = 300 K	11603	18051	23342	24561
T = 580 K	15705	21074	23952	24470
T = 900 K	14022	19803	23335	24013
T = 1100 K	11636	17817	22584	23634

(b) with fiber direction $[45/-45]_s$

a/h	**10**	**20**	**50**	**100**
T = 300 K	11320	17870	23495	24833
T = 580 K	15920	21483	24505	25052
T = 900 K	14259	20342	24157	24899
T = 1100 K	11842	18339	23527	24696

Table 5. Verification Critical temperature with different thickness ratio h_c/h

Cases	h_c/h			
Results	0.5	0.85	0.9	0.95
Present	0.05549	0.08152	0.08823	0.09528
Ref. [8]	0.05238	0.07954	0.08667	0.09498

Table 6. Critical temperature VS aspect ratio with different heat conditions

Cases	a/h			
Results	20	50	80	100
Uniform	9.911	9.908	7.897	5.210
Heat conduction	15.23	15.21	8.133	5.312

Table 7. Critical temperature with T-D SCF and TID SCF under heat conduction

Cases	a/h			
Results	20	50	80	100
T- D SCF	9.911	9.908	7.897	5.210
TID SCF	15.23	15.21	8.133	5.312

Table 8. Critical temperatures with different aerodynamic loads and SCF

Cases	λ			
a/h = 20	0	400	600	1000
T-D SCF	9.911	16.59	26.63	63.96
TID SCF	15.22	19.41	24.98	46.75

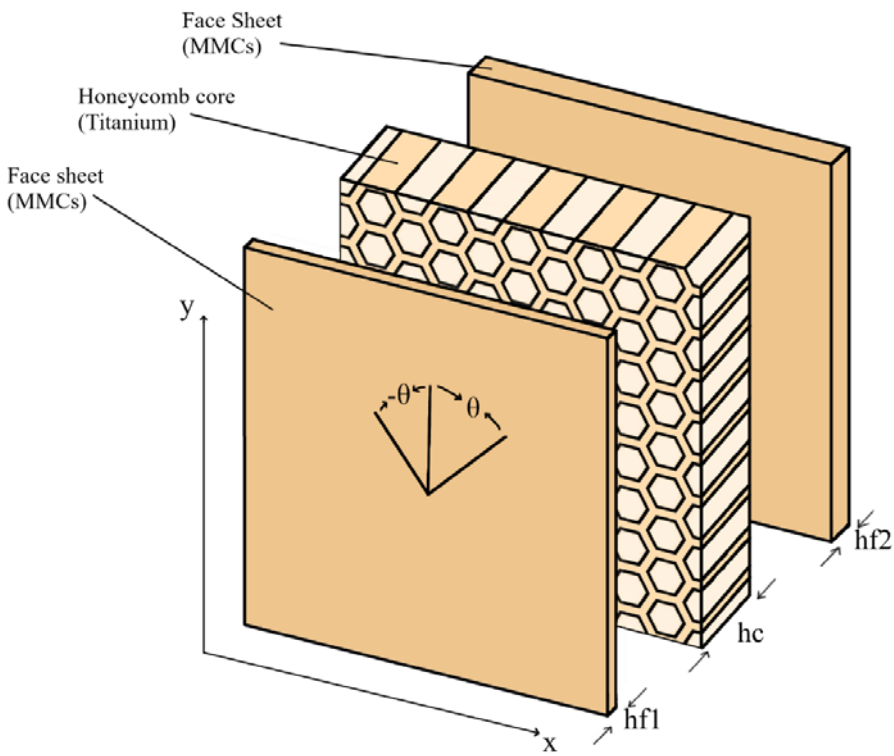

Fig. 1 Sandwich panel with MMC face sheet and titanium honeycomb core

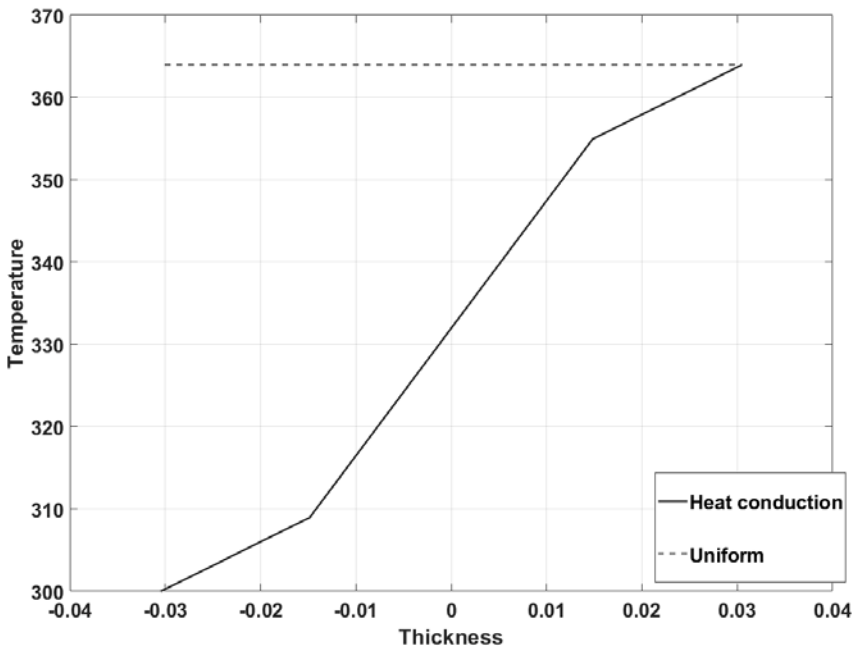

Fig. 2 Temperature difference with uniform case and heat conduction

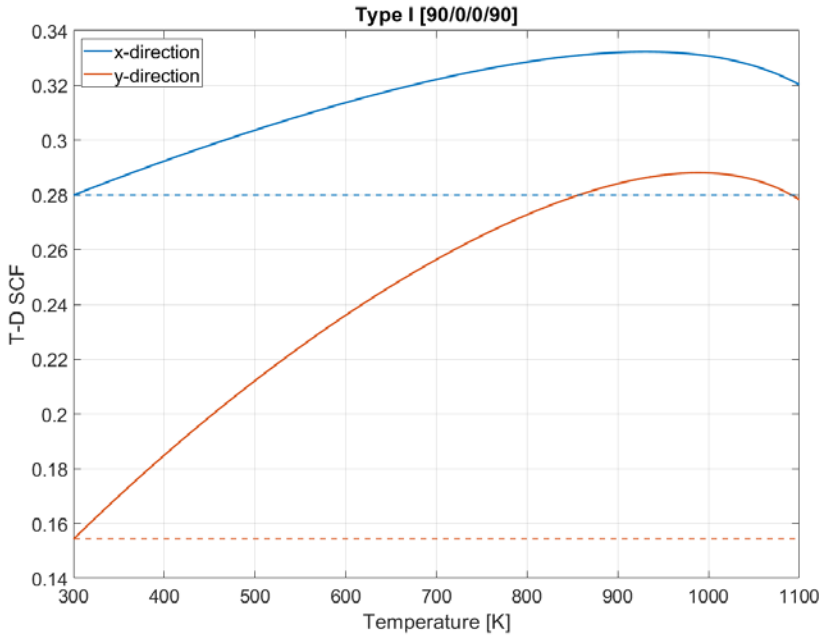

(a) with fiber direction $[90/0]_s$

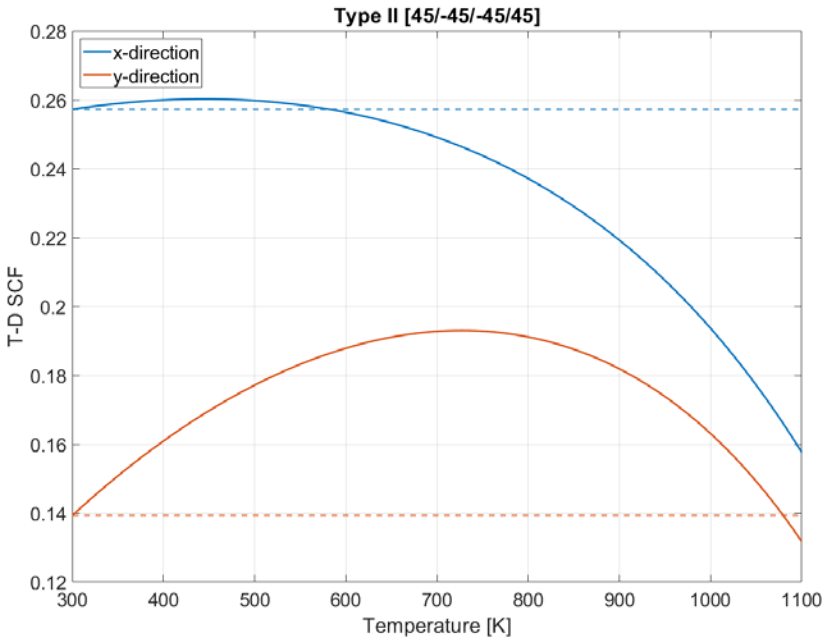

(b) with fiber direction $[45/-45]_s$

Fig. 3 Shear correction factor change due to temperature rise in x and y direction

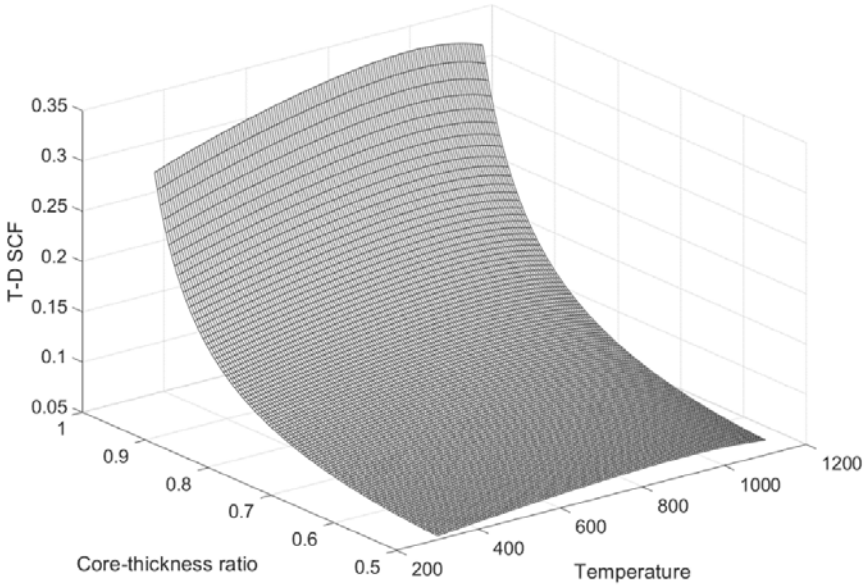

(a) with fiber direction $[90/0]_s$

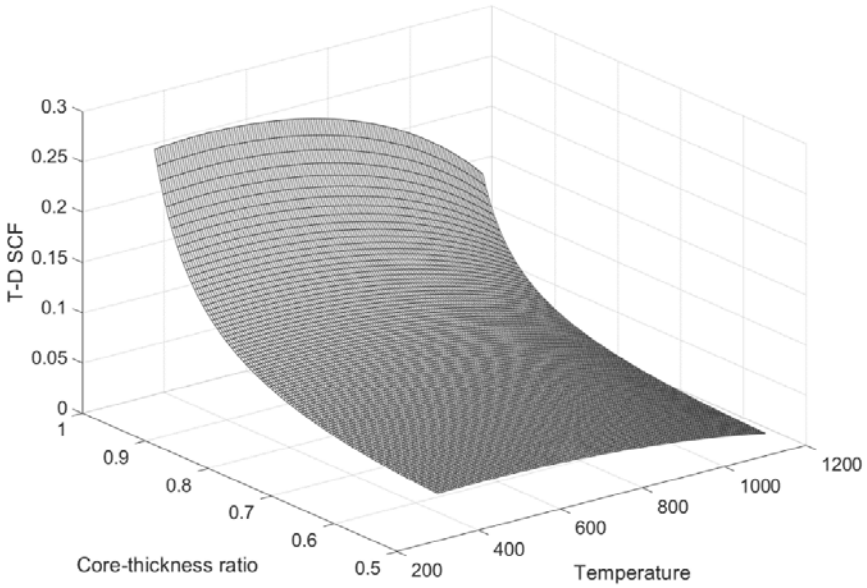

(b) with fiber direction $[45/-45]_s$

Fig. 4 Shear correction factor variation with the core-to-total thickness ratio

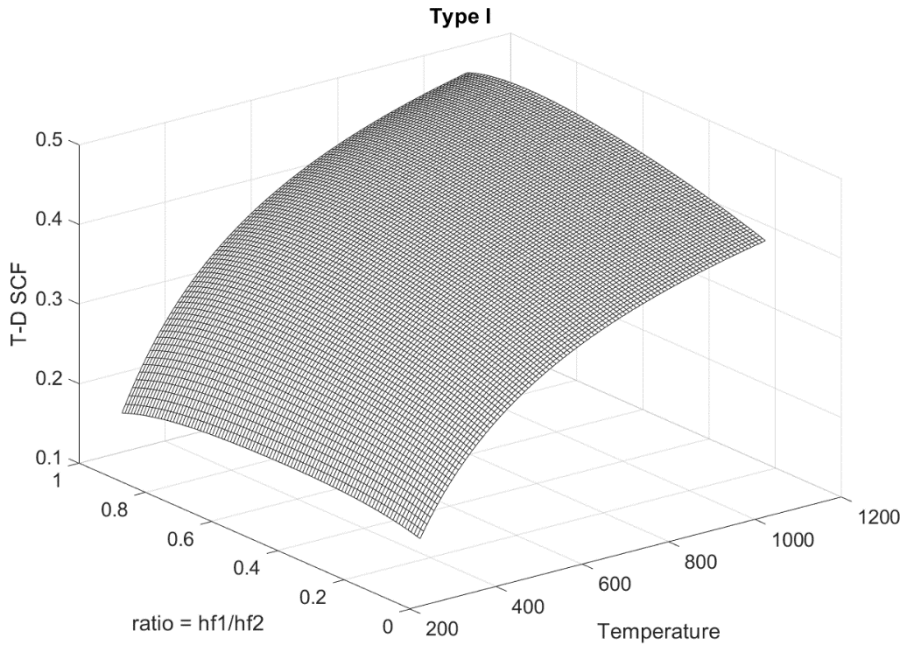

(a) with fiber direction $[90/0]_s$

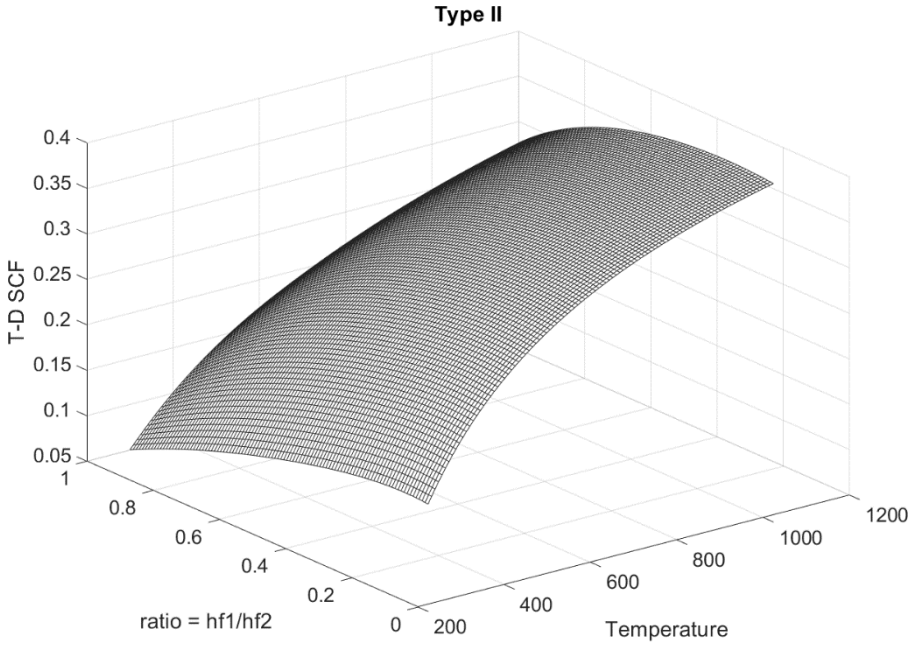

(b) with fiber direction $[45/-45]_s$

Fig. 5 Shear correction factor variation with the face sheet thickness ratio

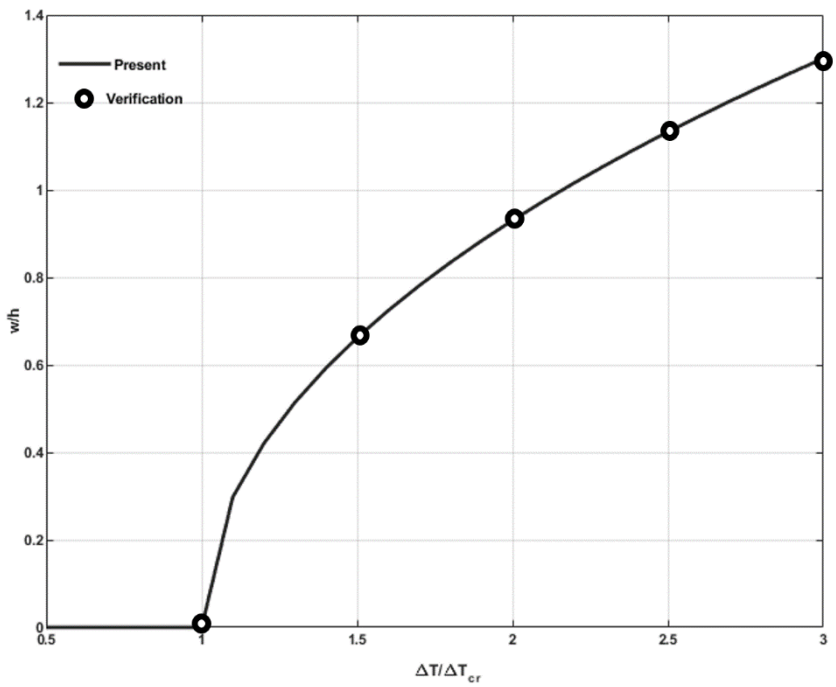

Fig. 6 Verification of Center deformation of the model with uniform temperature [43]

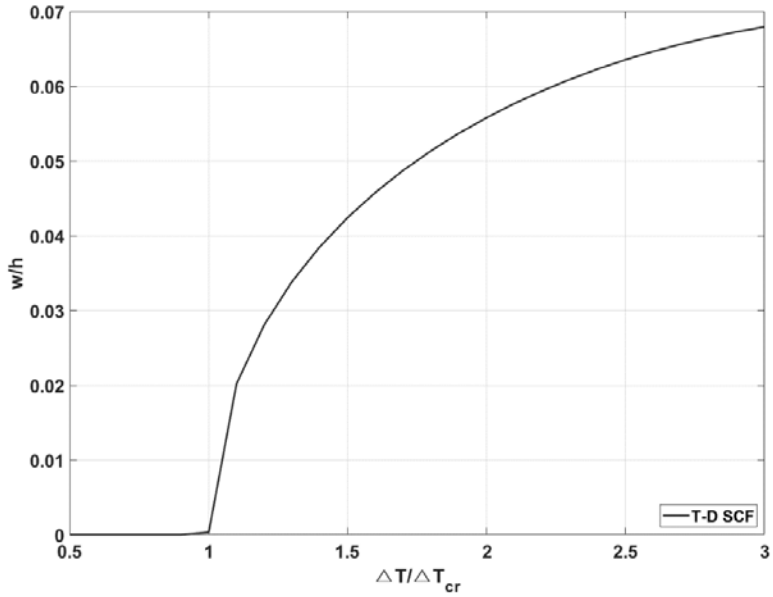

(a) with T-D SCF

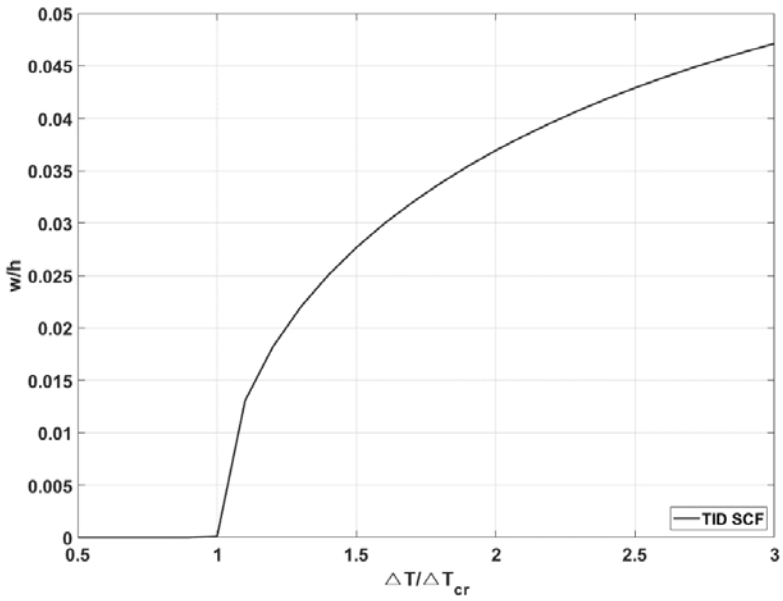

(b) with TID SCF

Fig. 7 Thermal post buckling analysis

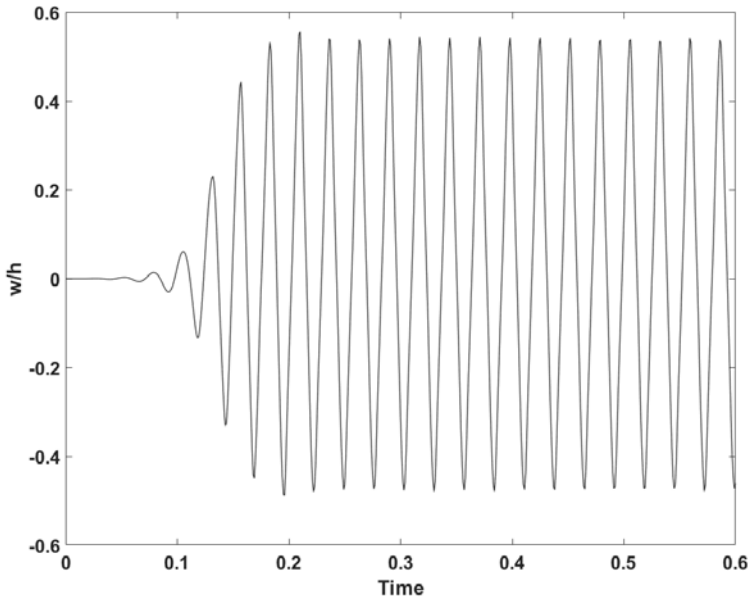

(a) Uniform temperature

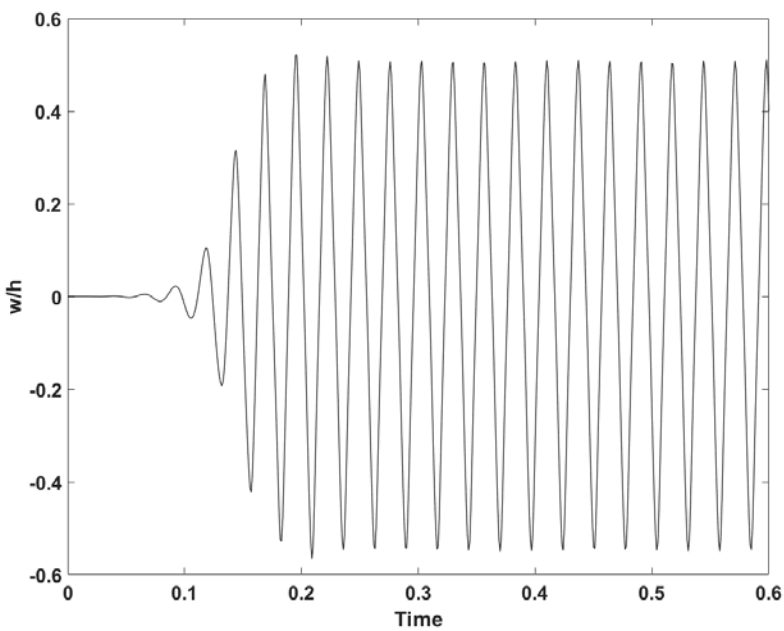

(b) Heat conduction

Fig. 8 Flutter behavior with uniform vs heat conduction

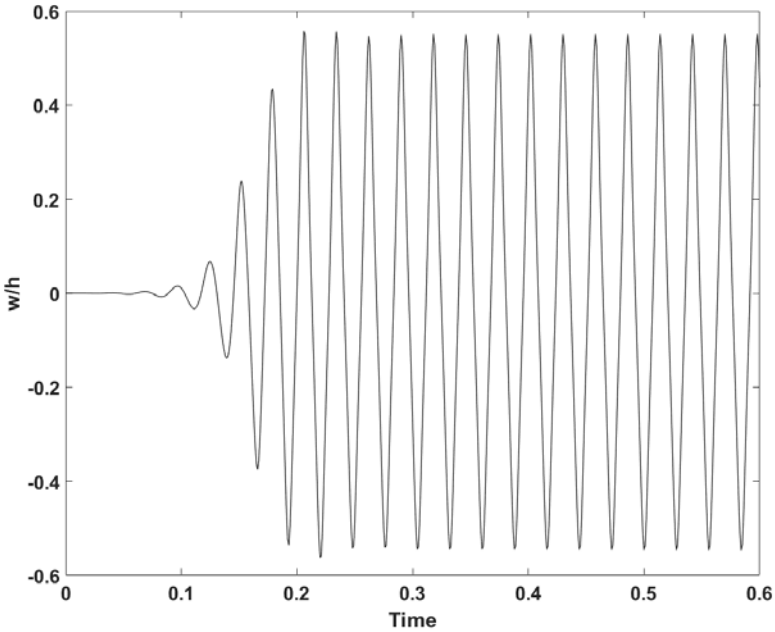

(a) T-D SCF

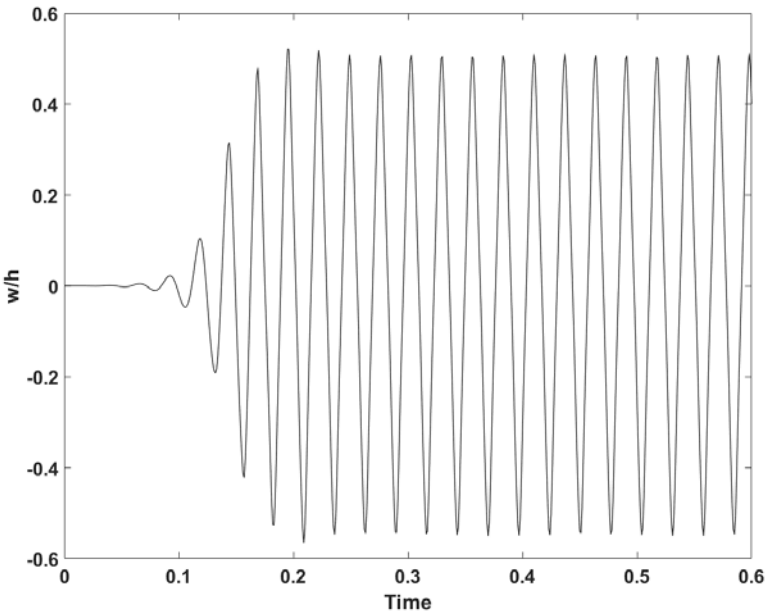

(b) TID SCF

Fig. 9 Flutter behavior with T-D vs TID SCF

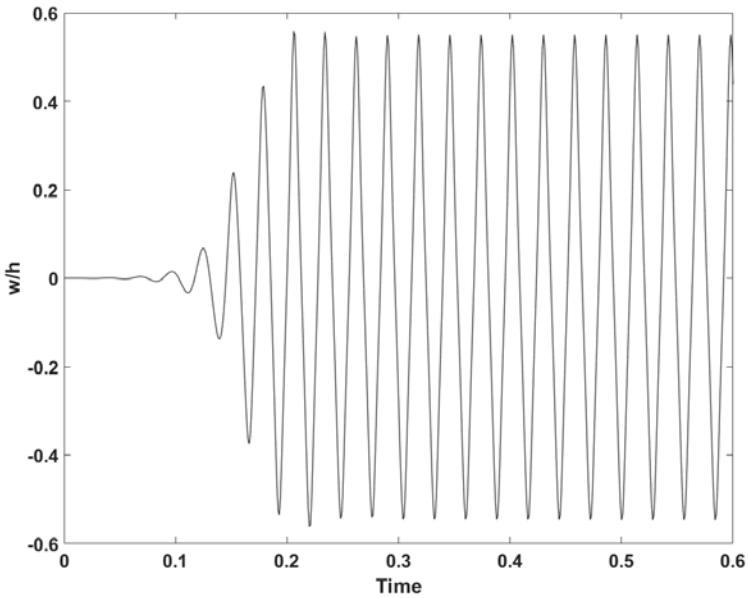

(a) $\Delta T = \Delta T_{cr}$

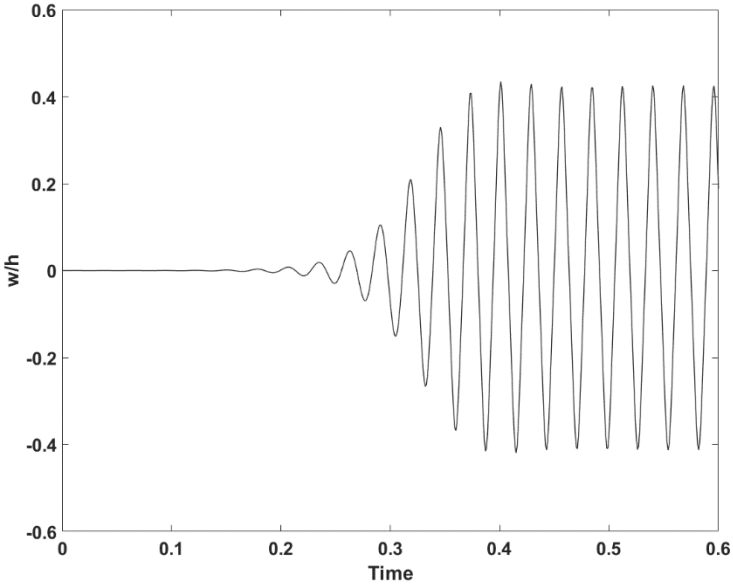

(b) $\Delta T = 0.1 * \Delta T_{cr}$

Figure. 10 Flutter behavior with T-D SCF under different temperature conditions

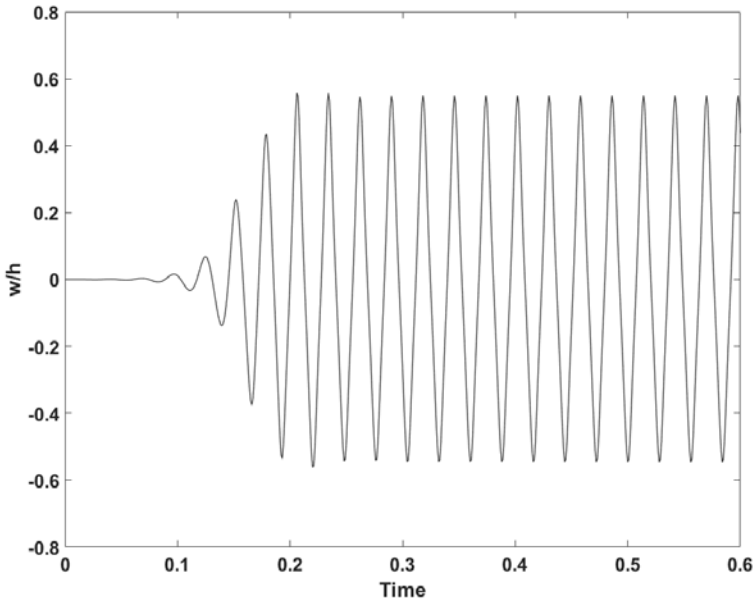

(a) λ = 1400

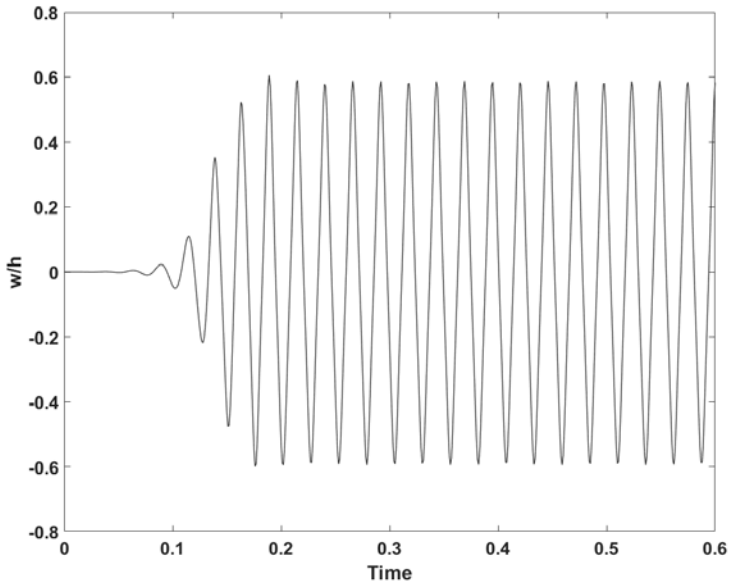

(b) λ = 1600

Figure. 11 Flutter behavior with T-D SCF under different dynamic pressure

Appendix A.

Temperature-dependent Shear Correction Factor

In the following, the detailed derivation process for the temperature-dependent shear correction factor is given. Strain energy equality is used to derive the equations, and the temperature-dependent material properties are considered for the SCF.

1. Shear correction factor in constitutive equation

The transverse shear stress resultant is derived by considering the constitutive relation for the transverse shear stress in a laminate plate:

$$\begin{Bmatrix} \tau_{yz}(T) \\ \tau_{xz}(T) \end{Bmatrix} = \begin{bmatrix} Q_{44}(T) & 0 \\ 0 & Q_{55}(T) \end{bmatrix} \begin{Bmatrix} \gamma_{yz}(T) \\ \gamma_{xz}(T) \end{Bmatrix} \tag{A-1}$$

where $Q_{44} = G_{yz}$ and $Q_{55} = G_{xz}$

The integration of Eq. (A-1) through the thickness of laminate plate yields

$$\begin{Bmatrix} Q_y(T) \\ Q_x(T) \end{Bmatrix} = \begin{bmatrix} \kappa_2(T)A_{44}(T) & 0 \\ 0 & \kappa_1(T)A_{55}(T) \end{bmatrix} \begin{Bmatrix} \gamma_{yz}(T) \\ \gamma_{xz}(T) \end{Bmatrix} \tag{A-2}$$

where $\{A_{44}(T), A_{55}(T)\} = \int_{-\frac{h}{2}}^{\frac{h}{2}} \{Q_{44}(T), Q_{55}(T)\} dz$, and $\kappa_1(T), \kappa_2(T)$ are the shear correction factors for *x* and *y* directions, respectively. The factor is accounted for the fact that τ_{xz} is not constant over the height of the section. Note that the factors are T-D, and the detailed derivation process is shown in the following section.

2. Detailed process

For the first step to derive the T-D SCF, consider the laminate composite plate shown in Fig. 1. From the FSDTP, the model is assumed to have a constant shear stress without the temperature in the thickness direction. The factor is derived from the strain energy equality, and since the calculating process of κ_1 and κ_2 for the plate are the same, the equation of κ_1 is shown in this section.

For the equilibrium equation including thermal effect for laminae are:

$$\sigma_{ij,j}(T) = 0, \quad \sigma_{zz} = 0 \quad (i, j = 1,2,3) \tag{A-3}$$

where σ_1, σ_2, and σ_3 are the normal and shear stresses in the x and y directions and the xy plane, respectively. Also, σ_{13} denotes τ_{xz}. Supposing the weak term without bending around *y*-axis, eq. (A-3) leads to

$$\sigma_{xx,x}(T) + \tau_{xz,z}(T) = 0 \tag{A-4}$$

From the definition of the in-place moment, known as a customary way:

$$\left(M_{\alpha\beta}\right)_T = \int_{-h/2}^{h/2} \sigma_{\alpha\beta}(z - z_N)dz \quad (\alpha, \beta = x, y) \tag{A-5}$$

then, σ_{xx} can be expressed as

$$\sigma_{xx}(z, T) = \frac{M_x Q_{11}(z, T)(z - z_{N1})}{D_{11}} \tag{A-6}$$

Substituting equation (A-6) into equation (A-4) and integrating with respect to the thickness direction:

$$\tau_{xz}(z,T) = -\int_{-h/2}^{z} \frac{\partial \sigma_{xx}(z,T)}{\partial x} \; dz \tag{A-7}$$

and using the defined neutral surface condition in equation (2), equation (A-7) turns into the following expression in [44]:

$$\tau_{xz}(z,T) = \frac{Q_x g(z,T)}{D_{11}} \tag{A-8}$$

where $g(z,T)$ denotes

$$g(z,T) \; = -\int_{-\frac{h}{2}}^{z} Q_{11}(z,T)(z - z_N)dz \tag{A-9}$$

Meanwhile, for the plate strain energy component is:

$$\int_{-h/2}^{h/2} \tau_{xz}\gamma_{xz} dz = \frac{Q_x^2}{\kappa_1(T) \int_{-\frac{h}{2}}^{\frac{h}{2}} G_{xz}(z,T)dz} \tag{A-10}$$

by integrating eq. (A-8) into the left side, equation (A-10) can be also expressed as the following

$$\int_{-h/2}^{h/2} \frac{\tau_{xz}^2}{G_{xz}(z,T)} dz = \frac{Q_x^2}{D_{11}^2} \int_{-h/2}^{h/2} \frac{g^2(z,T)}{G_{xz}(z,T)} dz \tag{A-11}$$

Finally, the T-D SCF is obtained by equaling eq. (A-10) t0 eq. (A-11):

$$\kappa_1(T) = \frac{D_{11}^2(z,T)}{\int_{-h/2}^{h/2} G_{xz}(z,T)dz \int_{-\frac{h}{2}}^{\frac{h}{2}} \frac{g^2(z,T)}{G_{xz}(z,T)} dz} \tag{A-12}$$

국 문 초 록

첨단 복합 구조물은 항공우주, 군사, 원자로, 화학 공장 및 현대 건축에 사용된다. 특히, 벌집 코어를 갖는 샌드위치 패널은 고온 지역에서의 사용을 위해 개발되어왔다. 증가된 온도가 복합구조물의 재료 특성에 영향을 미치면서 코어-외피 두께 비가 다른 열탄성 진동, 열 좌굴, 포스트-버클링 및 제한주기진동(LCO) 분석을 위한 비대칭 적층 복합판 모델이 해석되었다. 전단 보정 계수(SCF)를 채택한 판의 1차 전단 변형 이론(FSDTP)은 열 전도와 초음속 흐름을 고려하여 사용된다. SCF를 도출하기 위해 온도 의존적(T-D) 재료 특성을 이용하여 응력평형방정식에서 각 층과 복합판의 전단변형에너지 동일성을 이용하였다. 고온에서의 적용을 위해 MMC(Metal Matrix Composite)와 티타늄 벌집으로 구성된 페이스 시트와 코어를 갖는 3층 복합 모델이 도입됐다. 선형 분석의 경우 진동 및 열좌굴 분석을 위해 자연 주파수와 임계 온도가 각각 도출된다. 또한, 비선형 해석은 포스트-버클링을 위한 Newton-Raphson 반복계산법과 제한 주기 진동을 위한 Newmark 시간 반복 방법을 사용하여 수행된다. 1차 피스톤 이론은 공기 역학 부하에 대해 고려된다. 다양한 코어-페이스 시트 두께 비율, 종횡비 및 두가지 섬유 방향에 대한 다양한 사례 연구가 진행되고 있다. 결과는 기존 SCF를 사용하여 얻은 결과와 비교된다.

주요어: 온도 의존 특성, 열 전도, 공기역학, 중립면, 금속-매트릭스 혼

합물, 티타늄 벌집 구조

학 번: 2020-21216